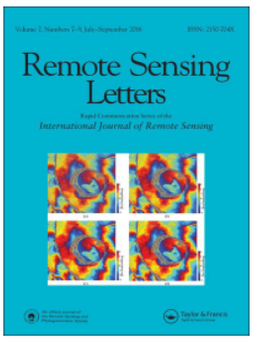

Remote Sensing Letters

ISSN: (Print) (Online) Journal homepage: https://www.tandfonline.com/loi/trsl20

A modified EMD method for detecting and mitigating narrow-band RFI in SAR data

Ning Li, Bingxu Chen, Zongsen Lv & Gaofeng Shu

To cite this article: Ning Li, Bingxu Chen, Zongsen Lv & Gaofeng Shu (2022) A modified EMD method for detecting and mitigating narrow-band RFI in SAR data, Remote Sensing Letters, 13:7, 643-650, DOI: 10.1080/2150704X.2022.2065894

To link to this article: https://doi.org/10.1080/2150704X.2022.2065894

Published online: 24 Apr 2022.

REMOTE SENSING LETTERS
2022, VOL. 13, NO. 7, 643–650
https://doi.org/10.1080/2150704X.2022.2065894

Taylor & Francis
Taylor & Francis Group

A modified EMD method for detecting and mitigating narrow-band RFI in SAR data

Ning Li[a,b,c], Bingxu Chen[a,b,c], Zongsen Lv[a,b,c] and Gaofeng Shu[a,b,c]

[a]College of Computer and Information Engineering, Henan University, Kaifeng, China; [b]Henan Key Laboratory of Big Data Analysis and Processing, Henan University, Kaifeng, China; [c]Henan Engineering Research Center of Intelligent Technology and Application, Henan University, Kaifeng, China

ABSTRACT

The empirical mode decomposition (EMD) based method for mitigating radio frequency interference (RFI) has the capability of removing narrow-band RFI and the advantage of easy-to-implement. The signals are decomposed by EMD into a finite number of intrinsic mode functions (IMFs) in a pulse-by-pulse manner, and then the IMFs corresponding to the RFI are subtracted to achieve interference mitigation. However, useful signals will be lost by using this method, which reduces the synthetic aperture radar (SAR) imaging quality. In this letter, a modified EMD method is proposed to tackle this problem. Firstly, the interferences of the echoes are detected through the relative energy ratio. Secondly, echoes containing RFI are decomposed into many IMFs via EMD. These IMFs are transformed into time-frequency (TF) domain via short-time Fourier transform (STFT), and then IMFs corresponding to RFI are screened out via the robust bisecting *k*-means algorithm. Finally, the RFIs in TF domain are located with the robust OTSU algorithm and mitigated by a notch operation. Experimental results of real SAR data with simulated RFIs demonstrate the effectiveness and superiority of the proposed method.

ARTICLE HISTORY
Received 30 September 2021
Accepted 6 April 2022

KEYWORDS
EMD; RFI; interference mitigation; SAR

1. Introduction

With the increasingly scarce electromagnetic spectrum resources, radio frequency interference (RFI) occurs more frequently (Tao et al. 2019). These interference signals will reduce the signal-to-interference and noise ratio of the synthetic aperture radar (SAR) image (Zhou et al. 2009), and appear as artefacts in the SAR image, resulting in blurring of the image.

The matrix decomposition method is regarded as an effective non-parametric interference mitigation method, including eigensubspace projection (Zhou et al. 2007), empirical mode decomposition (EMD) (Zhou et al. 2009), principal component analysis (Su et al. 2017), etc. The EMD method does not need to define the basis functions in advance, nor does it need to adopt the prior knowledge of this signal. Therefore, the EMD method has good adaptability and many applications in biomedicine (Tran et al. 2018) and remote sensing (Huang, Liu, and

CONTACT Gaofeng Shu gaofeng.shu@henu.edu.cn College of Computer and Information Engineering, Henan University, Kaifeng, 475004, China

Gill 2017) fields. The EMD-based method is easy to implement and robust to time-varying RFI (Zhou et al. 2009), thus it can be used to mitigate narrow-band RFI. However, a mass of valuable signals will be lost while using EMD method to mitigate interference.

In this letter, a modified EMD method is proposed. Firstly, interference detection is performed to identify echoes containing RFI via the relative energy ratio. Secondly, these echoes are decomposed by EMD into a series of intrinsic mode functions (IMFs). A robust bisecting *k*-means algorithm is applied to screen out IMFs corresponding to RFI. Thirdly, positions of RFI are located with the OTSU algorithm and RFIs are notched in time-frequency (TF) domain. The experimental results of measured SAR data with simulated RFIs verify the effectiveness of the method.

2. Basic theory

2.1. Short-Time Fourier transform

Short-time Fourier transform (STFT) is an established transform domain processing technology (Cai et al. 2021; Ede et al. 2021), and its principle is to map a one-dimensional signal into a two-dimensional function on the TF plane (Lyu et al. 2021). For a discrete time signal $S(s)$, STFT can be formulated as

$$X(m,n) = \sum_{s} \omega(m-s)S(s)\exp(-\mathrm{j}\pi sn/N) \tag{1}$$

where m, n, s and N denote time sample point, frequency sample point, signal integer index, and the total number of frequency sample point, respectively; ω denotes a sliding window; $S(s)$ denotes a discrete-time signal.

2.2. Empirical mode decomposition

The EMD method is a signal analysis method proposed by Huang et al. in (1998). The essence of this method is to decompose the fluctuations or trends of different scales in the signal gradually to obtain a series of sequences with different characteristic scales. Each sequence is called an IMF. A signal $x(t)$ can be decomposed by EMD as

$$x(t) = \sum_{i=1}^{N} \mathrm{IMF}_i(t) + r(t) \tag{2}$$

where N denotes the number of IMFs, $\mathrm{IMF}_i(t)$ denotes the ith IMF, $r(t)$ represents the mean or trend of the original data series.

3. Proposed method

In this letter, a modified EMD method is proposed. Compared with traditional EMD-based method, the proposed method has better mitigation performance. The flowchart of the proposed method is shown in Figure 1, where N_a denotes the number of samples in azimuth.

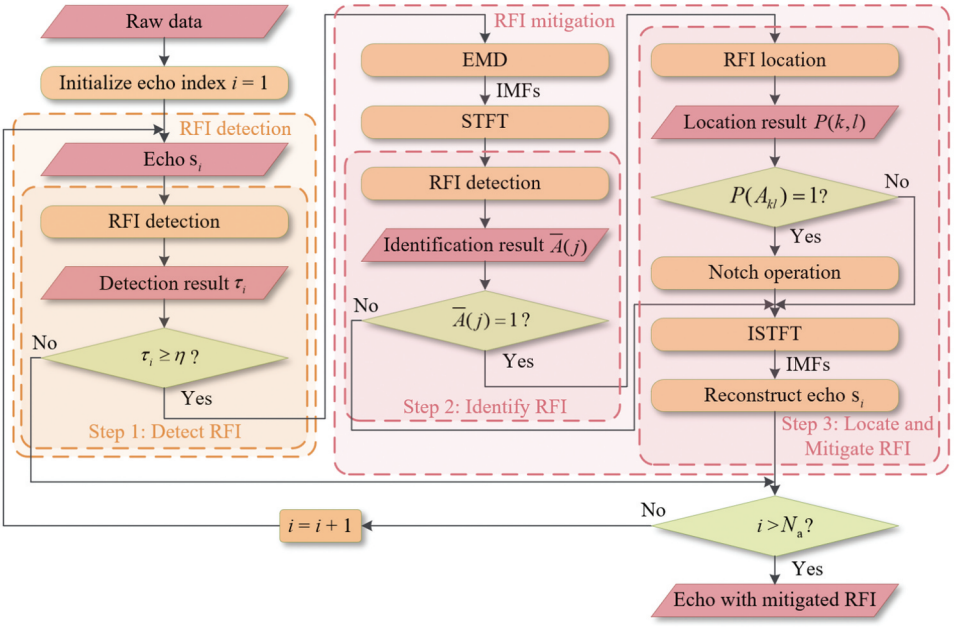

Figure 1. Flowchart of the proposed method.

3.1. RFI detection

To effectively mitigate RFI, a relative energy ratio method can be designed to detect whether RFI contaminates the echo data (Zhou et al. 2013). The relative energy ratio τ_i of the i-th echo s_i can be express as

$$\tau_i = \frac{\max[\mathrm{FT}(s_i)]}{E[\mathrm{FT}(s_i)]} \tag{3}$$

where $\max(\cdot)$ denotes the maximum value operation, $\mathrm{FT}(\cdot)$ denotes Fourier transform, and $E(\cdot)$ denotes the expectation operation. Then, it is divided into two situations. Situation I: s_i contains interference if τ_i is greater than or equal to the setting threshold. Situation II: s_i does not contain interference if τ_i is less than the setting threshold. Therefore, the criterion is

$$\begin{cases} \tau_i \geq \eta \Rightarrow \mathrm{SituationI} \\ \tau_i < \eta \Rightarrow \mathrm{SituationII} \end{cases} \tag{4}$$

The above operations are performed in a pulse-by-pulse manner. The threshold η is generally set between 2 and 10 (Zhou et al. 2013).

3.2. RFI mitigation

3.2.1. RFI identification

According to the RFI preliminary detection result, the echo containing RFI is decomposed into a finite number of IMFs through EMD, which can be expressed as

$$s_{i,\mathrm{RFI}} = \mathrm{IMF}_1 + \mathrm{IMF}_2 + \cdots + \mathrm{IMF}_N \tag{5}$$

where $s_{i,\mathrm{RFI}}$ denotes the echo s_i containing RFI, N denotes the total number of IMFs.

These IMFs are converted to TF domain via STFT, and then the amplitudes of their TF spectrums are taken into account. The TF spectrum of the n-th IMF can be expressed as

$$\mathrm{STFT}_{\mathrm{IMF}_n}(k,l) = \begin{bmatrix} A_{11} & A_{12} & \cdots & A_{1L} \\ A_{21} & A_{22} & \cdots & A_{2L} \\ \vdots & \vdots & A_{kl} & \vdots \\ A_{K1} & A_{K2} & \cdots & A_{KL} \end{bmatrix} \tag{6}$$

where IMF_n denotes the n-th IMF, $\mathrm{STFT}_{\mathrm{IMF}_n}$ denotes the TF spectrum of IMF_n. k, l, $K$and L denote time sample index, frequency sample index, the total number of time sample, and the total number of frequency sample, respectively. A_{kl} denotes one of the amplitudes of IMF_n in TF domain. The maximum amplitudes of IMFs in TF domain are considered to get the maximum amplitude sequences, which can be expressed as

$$A_{\max}(j) = [A_{\max,1} A_{\max,2} \ldots A_{\max,N}] \tag{7}$$

where $j = 1, 2, \ldots, N$, $A_{\max,j}$ denotes the maximum amplitude of the IMF_j in TF domain. The maximum amplitude sequence $A_{\max}(j)$ is divided into two categories via the robust bisecting k-means algorithm (Steinbach, George, and Vipin 2000). One type indicates that the corresponding IMFs contain RFI, and the other type indicates that the corresponding IMFs without RFI. α is obtained by bisecting k-means algorithm and defined as the threshold between the above two categories, and the threshold segmentation operation can be expressed as

$$\bar{A}(j) = \begin{cases} 1, A_{\max}(j) \geq \alpha \\ 0, A_{\max}(j) < \alpha \end{cases} \tag{8}$$

where $\bar{A}(j)$ denotes the detection result, the constants 1 and 0 represent the presence and absence of RFI, respectively.

3.2.2. RFI location and mitigation

According to $\bar{A}(j)$, the IMFs containing RFI are screened out. The OTSU algorithm is used to locate their RFI positions (Otsu 1979). The location results depend on the amplitude A_{kl} at the position (k, l) of IMF_n in TF domain and can be expressed as

$$P(A_{kl}) = \begin{cases} 1, A_{kl} \geq \xi \\ 0, A_{kl} < \xi \end{cases} \tag{9}$$

where the constants 1 and 0 represent the presence and absence of RFI, respectively. ξ is the segmentation threshold obtained by OTSU. Based on these positions, RFIs are accurately notched in TF domain. The notch process can be expressed as

$$\mathrm{STFT}_{\mathrm{IMF}_n}(k,l) = \begin{cases} 0, P(k,l) = 1 \\ \mathrm{STFT}_{\mathrm{IMF}_n}(k,l), P(k,l) = 0 \end{cases} \tag{10}$$

Next, the RFI-mitigated IMFs are transformed into time domain by ISTFT. Finally, all IMFs are summed up to reconstruct the target echo s_i, which can be expressed as

$$s_i = \overset{+}{\mathrm{IMF}}_1 \overset{+}{\mathrm{IMF}}_2 \cdots + \mathrm{IMF}_N \tag{11}$$

where IMF_n denotes IMF_n after RFI mitigation. The above operations are performed on all echoes containing RFI in a pulse-by-pulse manner. Compared with traditional EMD-based RFI mitigation methods, IMFs containing RFI are not totally subtracted by the proposed method but are notched in the TF domain. In this way, the signal loss after RFI mitigation is reduced to a small extent.

4. Experimental results

4.1. Results of simulated data

In order to verify the effectiveness of the proposed method, experiments with simulated data have been conducted. The main parameters of the simulation are summarized in Table 1. In the simulation, RFI with linear frequency modulation form is assumed. The RFI bandwidth B_{RFI} is 2%, 4%, 6%, 8%, and 10% of the SAR signal bandwidth.

As shown in Figure 2(a), the range peak sidelobe ratios (PSLR) of simulated point targets under five different B_{RFI} with four different methods are given. In Figure 2(a), it can be seen that more useful data is missed via frequency-domain notch filtering

Table 1. Main System Parameters of Simulation.

Parameters	Values
Carrier frequency	5.300 GHz
Sampling frequency	24 MHz
Efficient velocity	7100 ms^{-1}
Slant range	850,000 m
PRF	1700 Hz
Pulse width	40 μs
Pulse bandwidth	20 MHz
Carrier frequency of RFI	5.302 GHz
The amplitude ratio of RFI to signal	30
Bandwidth of RFI	.4 MHz, .8 MHz, 1.2 MHz, 1.6 MHz, 2 MHz

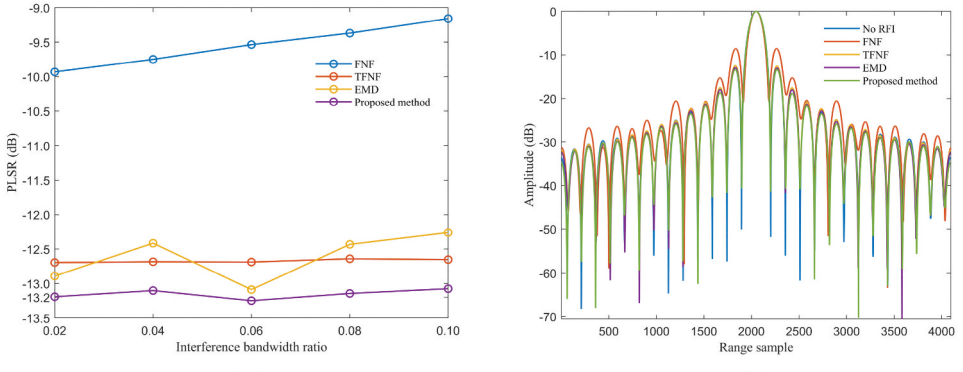

Figure 2. Mitigation performance analysis. (a) PSLR under different interference bandwidths. (b) Simulated point target range profile results where IBR is 2%.

(FNF), time-frequency-domain notch filtering (TFNF) and EMD method, which makes range PSLR worse. The proposed method significantly reduces the loss of useful data, and the range PSLR of the point target is closest to that of the ideal point target. With the increase of B_{RFI}, the range PSLR of point target progressively deteriorates and the RFI mitigation performance of all four methods is reduced. In Figure 2(b), the range profiles of four methods and the ideal point target are provided when the interference bandwidth ratio (IBR) is 2%. It can be seen that the side lobes of the proposed method are lower than those of the other three methods and are closest to those of the ideal point target, which agrees with the conclusion obtained from Figure 2(a).

4.2. Results of real SAR data with simulated RFIs

The experimental results of real SAR data with simulated RFIs are shown in Figure 3. The imaging result of raw data without RFIs and containing RFIs are given in Figure 3(a,c), respectively. The mitigation results of FNF, TFNF, EMD and the proposed method are shown in Figure 3(c–f), respectively. For a better comparison, in Figure 3(a–f) the areas marked by the yellow box are enlarged, as shown in Figure 3(g–l) respectively. It can be seen in Figure 3(i) that the strong target is defocused, which is due to the loss of a part of the useful spectrum using the FNF method. Figure 3(j,k) show the result of the TFNF and EMD method, respectively. They both lose some useful data, which cause an abnormal point target response. It can be seen in Figure 3(l) that the proposed method has a better mitigation effect.

The range profile and azimuth profile of the strong point target in Figure 3 are shown in Figure 4, and the average sidelobe energies in the azimuth and range, corresponding to Figure 4, are listed in Table 2. From the quantitative analysis of the results, it can be seen that the RFI mitigation effect of the proposed method is better than other methods.

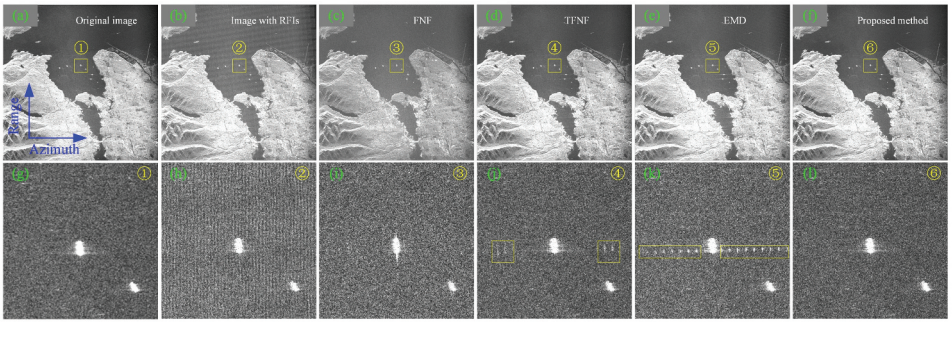

Figure 3. Experimental results for real SAR data with simulated RFIs. (a) The imaging result without RFIs. (b) The imaging result with RFIs. (c–f) Mitigation results by FNF, TFNF, EMD and proposed method, respectively. (g–l) Region of interest in (a-f) within yellow box, respectively.

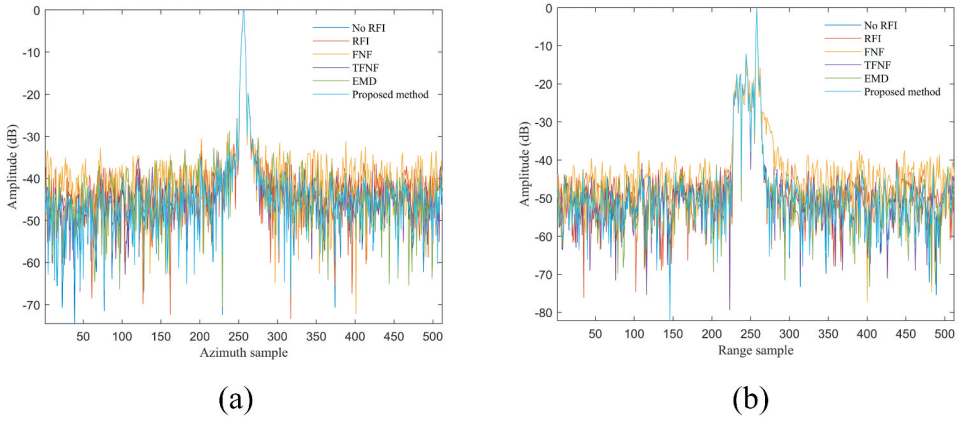

Figure 4. The profile of the strong point target. (a) The azimuth profile. (b) The range profile.

Table 2. The Average Sidelobe Energy in the Azimuth and Range.

Method	Energy values in the azimuth (dB)	Energy values in the range (dB)
No RFI	−46.9087	−51.1634
RFI	−44.2498	−48.8190
FNF	−40.6983	−46.6244
TFNF	−45.5764	−50.1787
EMD	−43.7358	−50.1343
Proposed Method	−46.7363	−51.0602

5. Conclusion

As a common form of SAR interferences, RFI is a problem that cannot be ignored in SAR system. In this paper, a modified EMD method for detecting and mitigating narrow-band RFI is proposed. The proposed method can more accurately mitigate RFI and retain useful signals as much as possible via three-step detection and location. In order to verify this method, experiments with simulated data and real SAR data containing simulated RFIs have been conducted. The experimental results show that the proposed method can effectively mitigate RFI and improve SAR imaging quality.

Disclosure statement

No potential conflict of interest was reported by the author(s).

ORCID

Ning Li http://orcid.org/0000-0002-4358-6449

References

Cai, J., H. Zhou, W. Huang, and B. Wen. 2021. "Ship Detection and Direction Finding Based on Time-Frequency Analysis for Compact HF Radar." *IEEE Geoscience and Remote Sensing Letters* 18 (1): 72–76. doi:10.1109/LGRS.2020.2967387.

Ede, B., B. Kaplan, I. Kahraman, S. Keşir, S. Yarkan, A. Ekti, T. Baykaş, A. Görçin, and H. Çırpan. 2021. "Independent Calculation of Move Lists for Incumbent Protection in a Multi-SAS Shared Spectrum Environment." *IEEE Wireless Communications Letters* 10 (1). Early access publication. doi:10.1109/LWC.2021.3122281.

Huang, N., Z. Shen, S. Long, M. Wu, H. Shih, Q. Zheng, N. Yen, C. Tung, and H. Liu. 1998. "The Empirical Mode Decomposition and Hilbert Spectrum for Nonlinear and Non-Stationary Time Series Analysis." *Proceedings of the Royal Society of London* 454 (1971): 903–995. doi:10.1098/rspa.1998.0193.

Huang, W., X. Liu, and E. Gill. 2017. "An Empirical Mode Decomposition Method for Sea Surface Wind Measurements from X-Band Nautical Radar Data." *IEEE Transactions on Geoscience and Remote Sensing* 55 (11): 6218–6227. doi:10.1109/TGRS.2017.2723431.

Lyu, Q., B. Han, G. Li, W. Sun, Z. Pan, W. Hong, and Y. Hu. 2021. "SAR Interference Suppression Algorithm Based on Low-Rank and Sparse Matrix Decomposition in Time-Frequency Domain." *IEEE Geoscience and Remote Sensing Letters*. Early access publication. doi:10.1109/LGRS.2020.3048161.

Otsu, N. 1979. "A Threshold Selection Method from Gray-Level Histograms." *IEEE Transactions on Systems, Man, and Cybernetics* 9 (1): 62–66. doi:10.1109/TSMC.1979.4310076.

Rilling, G., P. Flandrin, P. Goncalves, and J. M. Lilly. 2007. "Bivariate Empirical Mode Decomposition." *IEEE Signal Processing Letters* 14 (12): 936–939. doi:10.1109/LSP.2007.904710.

Steinbach, M., K. George, and K. Vipin. 2000. *A Comparison of Document Clustering Techniques*. Minneapolis: The University of Minnesota Digital Conservancy.

Su, J., H. Tao, M. Tao, L. Wang, and J. Xie. 2017. "Narrow-Band Interference Suppression via RPCA-Based Signal Separation in Time–frequency Domain." *IEEE Journal of Selected Topics in Applied Earth Observations and Remote Sensing* 10 (11): 5016–5025. doi:10.1109/JSTARS.2017.2727520.

Tao, M., J. Su, Y. Huang, and L. Wang. 2019. "Mitigation of Radio Frequency Interference in Synthetic Aperture Radar Data: Current Status and Future Trends." *Remote Sensing* 11 (20): 2438. doi:10.3390/rs11202438.

Tran, T., V. Pham, C. Lin, H. Yang, Y. Wang, K. Shyu, W. Tseng, M. Su, L. Lin, and M. Lo. 2018. "Empirical Mode Decomposition and Monogenic Signal-Based Approach for Quantification of Myocardial Infarction from MR Images." *IEEE Journal of Biomedical and Health Informatics* 23 (2): 731–743. doi:10.1109/JBHI.2018.2821675.

Zhou, F., R. Wu, M. Xing, and Z. Bao. 2007. "Eigensubspace-Based Filtering with Application in Narrow-Band Interference Suppression for SAR." *IEEE Geoscience and Remote Sensing Letters* 4 (1): 75–79. doi:10.1109/LGRS.2006.887033.

Zhou, F., M. Xing, X. Bai, G. Sun, and Z. Bao. 2009. "Narrow-Band Interference Suppression for SAR Based on Complex Empirical Mode Decomposition." *IEEE Geoscience and Remote Sensing Letters* 6 (3): 423–427. doi:10.1109/LGRS.2009.2015340.

Zhou, F., M. Tao, X. Bai, and J. Liu. 2013. "Narrow-Band Interference Suppression for SAR Based on Independent Component Analysis." *IEEE Transactions on Geoscience and Remote Sensing* 51 (10): 4952–4960. doi:10.1109/TGRS.2013.2244605.